
The Effect of Increased Irradiation Uniformity on Imprinting by 351-nm Laser Light

The experimental program¹ at LLE supports the national inertial confinement fusion (ICF) effort by performing experiments on OMEGA² to investigate the requirements for attaining ignition using direct-drive targets on the National Ignition Facility. One of the primary challenges in direct-drive ICF is to minimize perturbations in the target that are created by nonuniformities in the drive laser. These imprinted perturbations can seed the Richtmeyer–Meshkov (RM) and Rayleigh–Taylor (RT) instabilities that can amplify target nonuniformities sufficiently large enough to destroy an implosion. Typical high-gain implosions are expected to experience unstable growth factors in excess of 500.

One of the primary experimental efforts is to reduce imprinting by controlling irradiation nonuniformities. Other methods being studied include modifications to the target (foam buffers) and general reduction of growth rates; these methods will be reported on in the future. Eventually, successful ICF implosions may require some level of each of these methods. Here, we report on planar-target experiments that quantify the effect of changes to irradiation nonuniformity on imprinting. In addition, we report on “perturbing-beam” experiments—a novel method to measure the times over which imprinting occurs.

Drive nonuniformities conventionally are expressed in terms of spherical-harmonic ℓ -modes that describe the number of perturbation wavelengths contained in the circumference of a spherical target. The amplitudes of the low-order modes ($\ell \leq 8$) are affected by the configuration, pointing, and focusing of the beams, and by beam-to-beam power balance. In contrast, imprinting occurs predominantly in the high-order modes ($\ell \geq 8$), which largely result from nonuniformities in the intensity distributions of the individual beams. To reduce these nonuniformities, beam-smoothing techniques for glass lasers have traditionally relied on the physical optics associated with optical arrays placed in each of the laser beams. Distributed phase plates³ (DPP’s) act to randomize the phase across the beam wavefront, producing a speckle pattern with high-frequency modulations. Smoothing by spectral dispersion⁴ (SSD)

produces a variable frequency across the wavefront, producing multiple modes that are displaced in the target plane and, when averaged over time, smooth the DPP speckle nonuniformities. The DPP’s transform the long-wavelength beam nonuniformities (typical of high-power lasers) to wavelengths sufficiently short enough that displacements of the speckle pattern (caused by SSD) smooth out most of the nonuniformities.

Distributed polarization rotators⁵ (DPR’s) change the beam polarization across the wavefront (and therefore across the DPP), thereby diminishing the interference responsible for the high-frequency modulations in the DPP pattern. Since beams of orthogonal polarization do not interfere, the uniformity can be increased in proportion to the square root of the number of polarization states one produces in the wavefront, which in the case of the current DPR’s is 2.

To assess the irradiation uniformity, equivalent-target-plane (ETP) images of single beams with various beam-smoothing techniques have been analyzed. Beams with (1) DPP’s only, (2) DPP and 1-D SSD (1.5 Å), and (3) DPP and 2-D SSD (0.6 Å × 1.5 Å) were compared and, when measured over the duration of a 1-ns pulse, had time-averaged nonuniformities of 98%, 25%, and 12%, respectively.⁶ A recent implementation of DPR’s for OMEGA is shown in Fig. 71.1. A wedge of KDP (a birefringent material) is inserted such that the beam polarization bisects the ordinary and extraordinary axes. Since the element is wedged, the two orthogonally polarized beams emerge from the KDP at different angles, thereby producing two speckle patterns that are shifted by $\approx 80 \mu\text{m}$ [see Fig. 71.1(a)]. Since the two beams are orthogonally polarized, the two speckle patterns do not interfere and, therefore, produce a $1/\sqrt{2}$ ($N = 2$ beams) reduction in nonuniformity. This increase occurs instantaneously and is therefore particularly important to direct drive because irradiation imprinting occurs early in the drive and in some cases before appreciable SSD smoothing takes place. Figure 71.1(b) compares the uniformity of single beams with DPP’s only (i.e., no SSD), with and without DPR’s. To produce these plots, the square of the Fourier transform of the ETP images is integrated azimuthally

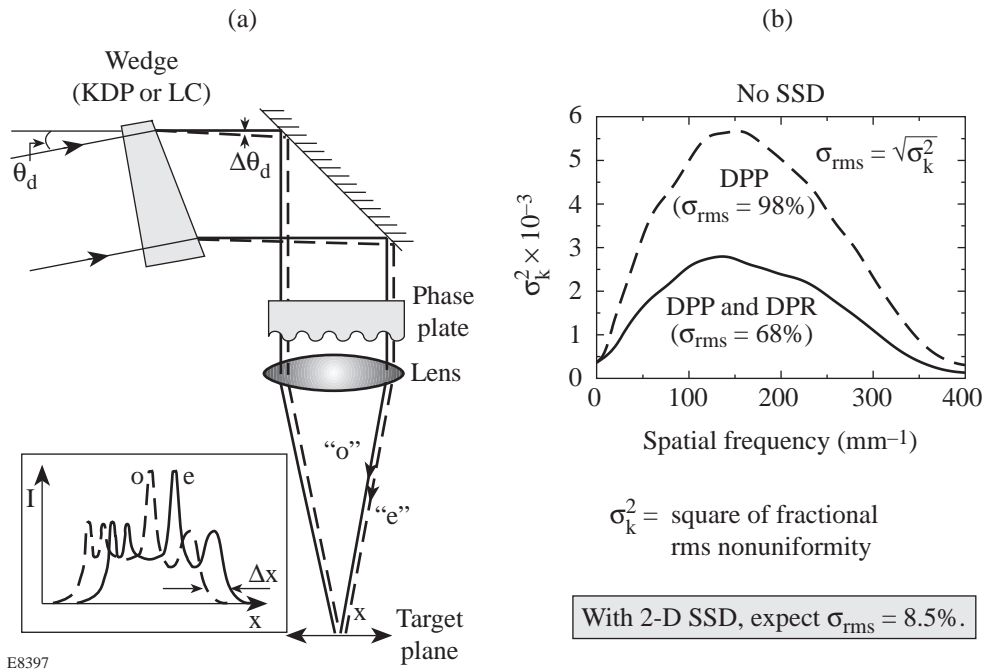


Figure 71.1
 (a) Schematic of a DPR (a KDP wedge in the initial implementation on OMEGA) and (b) nonuniformity spectrum on target with and without DPR's for an OMEGA beam with phase plates (DPP's) but no SSD.

at constant radii, i.e., constant spatial frequency. The graphs are the square of the contribution (σ_k^2) to total nonuniformity as a function of spatial frequency. (The upper limit in frequency is the diffraction limit of the OMEGA lenses.) These graphs indicate that the $1/\sqrt{2}$ factor applied to σ_{rms} for the 2-D SSD result (above) should produce a time-integrated uniformity of 8.5% rms. Contributions to nonuniformity from film noise prevented this comparison from being performed on the 2-D SSD beams. We expect to use electronic imaging to further study the highly uniform beams.

Imprinting Experiments

Several multifoil, planar-target experiments were performed on OMEGA to study hydrodynamic instabilities. These experiments, which began on Nova as a collaboration between Lawrence Livermore National Laboratory (LLNL) and LLE,⁷ study two aspects of direct-drive target stability: growth rates and irradiation imprinting. Using x-ray radiography, the target trajectories and the growth of pre-imposed mass perturbation were measured in accelerated targets. These experiments were well simulated by hydrocodes, providing confidence that both the energy coupling⁸ and unstable growth⁹ are well modeled for these experiments. This confirmed our experience in similar experiments conducted on Nova.

The effect of irradiation nonuniformity on laser imprinting was studied using unperturbed CH₂ targets driven by five overlapped UV beams at 2×10^{14} W/cm² in 3-ns square

pulses. The targets were backlit with x rays produced by a uranium backlighter irradiated at $\sim 2 \times 10^{14}$ W/cm² (using 12 beams). X rays transmitted through the target were imaged using a framing camera with 8- μm pinholes filtered with 20 μm of Be and 12 μm of Al. This yielded highest sensitivity at an average photon energy of ~ 1.3 keV. Face-on radiographic images at different times were analyzed to measure the growth of perturbations seeded by imprinting. Since the initial perturbations are too small to be detected by this method, RT growth (driven by the target acceleration) is employed to amplify the imprint perturbations to detectable levels. Unfortunately, the addition of this highly nonlinear “amplifier” somewhat complicates interpretation of the results.

Figure 71.2 shows a series of radiographic images taken at 2.4 ns for each of four different laser configurations (all with DPP's): (a) no SSD, (b) 1-D SSD (1.5 Å), (c) 2-D SSD (0.6 Å \times 1.5 Å), and (d) DPR's and 2-D SSD (0.6 Å \times 1.5 Å). These configurations are listed in order of increasing on-target uniformity, which can be estimated by multiplying the time-integrated single-beam nonuniformities by $1/\sqrt{5}$ ($N=5$ beams), yielding 44%, 11%, 5.4%, and 3.8%, respectively, for the four configurations. Note, however, that at time equals zero, the first three cases present identical nonuniformities (i.e., the DPP speckle patterns) to the target. As time progresses, SSD provides time-averaged smoothing, the level of which depends upon the degree of SSD (bandwidth and number of dimensions). In contrast, the DPR's provide a $1/\sqrt{2}$ increase in

uniformity instantaneously (at time zero and all times) because two speckle patterns (from each beam) are continuously incident on the target.

Figure 71.3 depicts the nonuniformity “power spectra” obtained at different times from radiographic images of targets irradiated with various laser configurations. The spectra for the images in Fig. 71.2 (at 2.4 ns) are the top line in each graph. An estimate of the noise level for the diagnostic is shown as the gray regions. The nonuniformities depicted by these graphs result from acceleration-driven growth that is seeded by imprinting. Each point in these graphs is the azimuthal integral at constant radius (constant frequency) of the two-dimensional Fourier transform of the radiographic images. The summation

of each graph over all frequencies provides the square of the total rms deviation from a smooth envelope, i.e., the nonuniformities in that image. Note that, at a given time, the nonuniformities in these images decrease as the irradiation uniformity is improved. Since the pulse shape and drive intensities were the same, the growth rates are expected to be similar for all cases. The higher uniformity of the accelerated targets is, therefore, indicative of lower initial perturbation amplitudes, i.e., less imprinting. The smallest amount of imprinting occurs for the case with 2-D SSD and DPR’s. Inferences of the actual imprint amplitudes will be made using hydrodynamic simulations that have been normalized using the growth-rate data and include instrument response functions and noise levels.

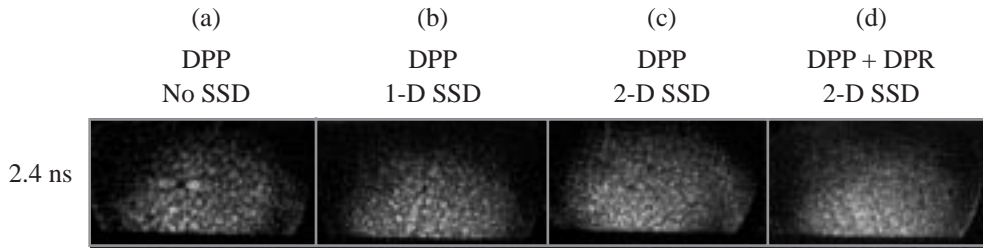


Figure 71.2 Radiographic images of 25- μm CH_2 foils taken at 2.4 ns and irradiated by 3-ns UV pulses having a variety of laser conditions (all with DPP’s): (a) no SSD, (b) 1-D SSD, (c) 2-D SSD, and (d) DPR’s and 2-D SSD. The latter images show higher uniformity of the accelerated target.

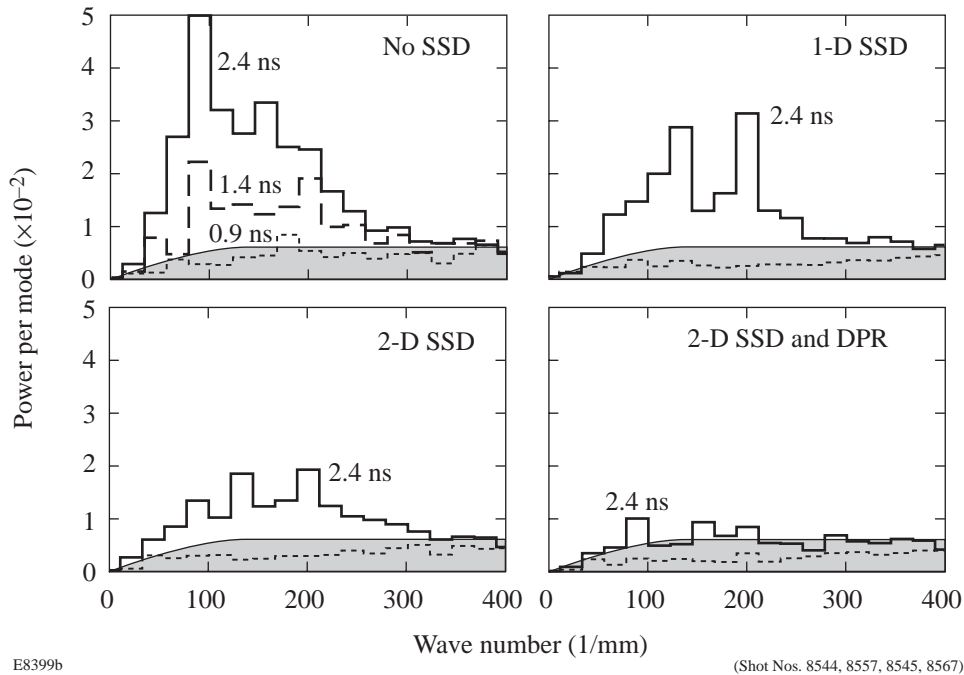


Figure 71.3 Measured nonuniformity power spectra of the x-ray backlighter transmission through accelerated CH foils subjected to a variety of laser-irradiation conditions. Fourier analysis of various x-ray framing camera images is shown for the times indicated. The maximum wave number shown (400 mm^{-1}) corresponds to a spatial wavelength of $16 \mu\text{m}$.

This analysis is performed on the optical depth of the target (the natural log of the intensity-converted images). Using calibration targets, it is estimated that ratios of local intensities in Fig. 71.2(a) indicate that many RT “bubbles” have nearly penetrated the foil. The power spectra belie this point because the Fourier amplitudes correspond to modulations of less than $1\ \mu\text{m}$. This is because the target nonuniformities comprise a wide range of frequencies, so the individual amplitudes are relatively small. (This is in contrast to the single-mode experiments where the images are dominated by the imposed modulations.) Furthermore, one cannot estimate growth rates by tracking the amplitudes of individual modes at various times because the radiographic contrast of these measurements is sufficiently low that a significant amount of RT growth (linear and possible nonlinear) is needed to observe the target nonuniformities. This implies that saturation and possibly mode competition and coalescence dramatically affect the shape of the power spectrum. (In fact, many of our results exhibit a shift to longer wavelengths for late times.) Also, the MTF of the device has not been included in the measurements; if it were, the noise-dominated signal at shorter wavelength would appear as a dominant factor. To properly analyze these experiments we are investigating other image-analysis techniques and will use hydrodynamic simulations that include the instrument response. This is particularly important for spatial wavelengths $20\ \mu\text{m}$ and lower.

The time dependence of imprinting is important for determining the requirements for beam-smoothing rates. Imprint-

ing occurs until sufficient coronal plasma is produced and laser nonuniformities (those with wavelength shorter than the distance from the critical to the ablation surfaces) are smoothed by that plasma. Simulations¹⁰ indicate that for pertinent ICF conditions, irradiation nonuniformities decouple from the ablation surface after 300 to 500 ps. As shown above, SSD reduces imprinting, yet the addition of DPR's shows continued reduction of imprinting. This indicates that imprinting occurs before this level of SSD smoothing is fully effective.

To understand the time over which imprinting occurs, a series of preliminary experiments were conducted on OMEGA before DPP's and SSD were available. In these experiments, five beams without DPP's accelerated initially smooth targets, and a sixth beam of smaller diameter was added at different times and with different energies. The relative effect of the sixth beam is gauged by observing the nonuniformities in the accelerated target. One can estimate the duration of imprinting by determining the perturbing-beam delay that no longer produces observable effects in the accelerated target.

For these experiments, the nominal drive beams were $1000\ \mu\text{m}$ in diameter and the perturbing beam was $400\ \mu\text{m}$. The drive intensity was $\sim 1 \times 10^{14}\ \text{W}/\text{cm}^2$ in 1-ns Gaussian pulses. Qualitatively, dramatic differences can be seen in the radiographic images for different conditions of the perturbing beam. Figure 71.4 depicts images from two shots with different timing of the perturbing beam. The upper images [Fig. 71.4(a)] show that, when timed 150 ps before the drive pulses, the

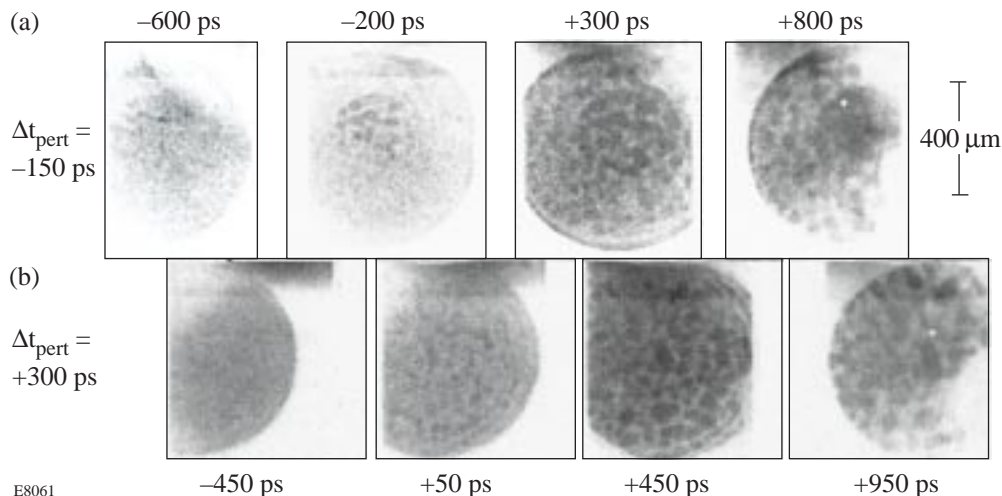


Figure 71.4

Framing camera images at various times relative to the peak of the Gaussian 1-ns drive beams for two shots: (a) perturbing beam at $-150\ \text{ps}$ and (b) perturbing beam at $+300\ \text{ps}$. The effect of the $400\text{-}\mu\text{m}$ -diam perturbing beam on the accelerated target uniformity is diminished when it arrives sufficiently late in time.

perturbing beam imprinted its features (smaller circle of nonuniformities) onto the target. The perturbing beam also produced similar effects when it was timed coincident (0 ps) with drive beams. Figure 71.4(b) shows the diminished effect of the perturbing beam when it is delayed by 300 ps with respect to the drive beams. This is likely the result of sufficient plasma formation (by the primary beams) to allow smoothing of the irradiation nonuniformities produced by the perturbing beam. In both cases, the perturbing beam had an intensity equal to the total drive-beam intensity, i.e., $\sim 1 \times 10^{14}$ W/cm². When the intensity of the perturbing beam was reduced to 7% of the drive beams' intensity, its effect was no longer observed in the radiographic images. The mottled patterns in Fig. 71.4 are the growth of features imprinted by the 1-mm drive beams. Similar features can be seen in the outer annulus of the images in Fig. 71.4(a). We expect that refinement of these experiments will provide insight into imprinting mechanisms and their time dependence, as well as provide information on the effectiveness of uniformity enhancements to the laser.

The next step in this effort will be to study the growth and mitigation of short-wavelength imprinting and to diagnose smaller amplitude perturbations. By relying less on the RT instability to amplify the perturbations, measurements performed at earlier times may provide better estimates of the spectrum and amplitude of imprinting. These measurements will require higher-resolution x-ray imaging ($<10 \mu\text{m}$) and higher-contrast measurements and will be attempted using a Kirkpatrick–Baez microscope or curved-crystal x-ray imaging, and high-resolution imaging of a 250-eV backlighter. In addition, imprint mitigation and growth-rate reduction will be studied using target modifications such as foam buffers and high-Z dopants.

Summary

The mitigation of the deleterious effects of laser imprinting in direct-drive ICF targets is crucial to LLE's experimental program. The primary approach—increased irradiation uniformity—has been shown to reduce imprinting levels, particularly for a new beam-smoothing device called distributed polarization rotator (DPR). The perturbing-beam experiments presented here demonstrate a novel way to study the time dependence of imprinting—an important issue for the design of certain uniformity schemes. To study imprinting earlier in time and perturbations with shorter wavelengths, we are investigating other diagnostics for radiography, including a number of advanced x-ray and XUV diagnostics.

ACKNOWLEDGMENT

This work was supported by the U.S. Department of Energy Office of Inertial Confinement Fusion under Cooperative Agreement No. DE-FC03-92SF19460, the University of Rochester, and the New York State Energy Research and Development Authority. The support of DOE does not constitute an endorsement by DOE of the views expressed in this article.

REFERENCES

1. R. L. McCrory, J. M. Soures, C. P. Verdon, T. R. Boehly, D. K. Bradley, R. S. Craxton, J. A. Delettrez, R. Epstein, P. A. Jaanimagi, S. D. Jacobs, R. L. Keck, J. H. Kelly, T. J. Kessler, H. Kim, J. P. Knauer, R. L. Kremens, S. A. Kumpan, S. A. Letzring, F. J. Marshall, P. W. McKenty, S. F. B. Morse, A. Okishev, W. Seka, R. W. Short, M. D. Skeldon, S. Skupsky, M. Tracy, and B. Yaakobi, in *Plasma Physics and Controlled Nuclear Fusion Research 1994* (IAEA, Vienna, 1996), Vol. 3, pp. 33–37.
2. T. R. Boehly, D. L. Brown, R. S. Craxton, R. L. Keck, J. P. Knauer, J. H. Kelly, T. J. Kessler, S. A. Kumpan, S. J. Loucks, S. A. Letzring, F. J. Marshall, R. L. McCrory, S. F. B. Morse, W. Seka, J. M. Soures, and C. P. Verdon, *Opt. Commun.* **133**, 495 (1997).
3. Y. Lin, T. J. Kessler, and G. N. Lawrence, *Opt. Lett.* **20**, 764 (1995); Laboratory for Laser Energetics LLE Review **65**, 1, NTIS document No. DOE/SF/19460-117 (1995). Copies may be obtained from the National Technical Information Service, Springfield, VA 22161.
4. S. Skupsky, R. W. Short, T. Kessler, R. S. Craxton, S. Letzring, and J. M. Soures, *J. Appl. Phys.* **66**, 3456 (1989).
5. Laboratory for Laser Energetics LLE Review **45**, 1, NTIS document No. DOE/DP40200-149 (1990). Copies may be obtained from the National Technical Information Service, Springfield, VA 22161.
6. T. Boehly, R. S. Craxton, P. A. Jaanimagi, R. L. Keck, J. H. Kelly, T. J. Kessler, R. L. Kremens, S. A. Kumpan, S. A. Letzring, R. L. McCrory, S. F. B. Morse, W. Seka, S. Skupsky, J. M. Soures, M. D. Tracy, and C. P. Verdon, in *Conference on Laser and Electro-Optics*, Vol. 9, 1996 OSA Technical Digest Series (Optical Society of America, Washington, DC, 1996), p. 324.
7. S. G. Glendinning, S. V. Weber, P. Bell, L. B. DaSilva, S. N. Dixit, M. A. Henesian, D. R. Kania, J. D. Kilkenny, H. T. Powell, R. J. Wallace, P. J. Wegner, J. P. Knauer, and C. P. Verdon, *Phys. Rev. Lett.* **69**, 1201 (1992).
8. D. D. Meyerhofer, J. P. Knauer, T. R. Boehly, D. Ofer, C. P. Verdon, P. W. McKenty, V. A. Smalyuk, O. Willi, and R. G. Watt, *Bull. Am. Phys. Soc.* **41**, 1480 (1996).
9. J. P. Knauer, D. D. Meyerhofer, T. R. Boehly, D. Ofer, C. P. Verdon, D. K. Bradley, P. W. McKenty, V. A. Smalyuk, S. G. Glendinning, and R. G. Watt, "Single-Mode Rayleigh-Taylor Growth-Rate Measurements with the OMEGA Laser System," to be published in the *Proceedings of the Thirteenth International Conference on Laser Interactions and Related Plasma Phenomena (LIRPP)*, Monterey, CA, 13–18 April 1997.
10. R. J. Taylor *et al.*, *Phys. Rev. Lett.* **76**, 1643 (1996).

